UMBC 73-19
UR-460

COO-3065-59

Pion Production in pp Collisions at 102 GeV/c*

C. Bromberg, D. Chaney, D. Cohen†, T. Ferbel‡, and P. Slattery

University of Rochester

Rochester, New York 14627
Contract Number AT(11-1)-3065

J. W. Chapman, J. W. Cooper, N. Green,

A. A. Seidl and J. C. Vander Velde

University of Michigan

Ann Arbor, Michigan 48104
November 9, 1973

We investigate single-pion production and two-pion correlations making use of a 30,000 picture exposure of the ANL/NAL 30-inch hydrogen bubble chamber to 102 GeV/c protons. The charge dependence of the correlations are presented.

*Research supported in part by the U.S. Atomic Energy Commission. Computing funds at the University of Rochester are provided by the University.

†Present Address: Nevis Laboratory, Columbia University
P.O. Box 137, Irvington-on-Hudson, N.Y. 10533

‡A. P. Sloan Fellow.

Submitted to Physical Review for publication.

We present an investigation of π^+ and π^- production in pp collisions at 102 GeV/c. The data are from the complete measurement of a film sample containing ~650 events and an additional 1200 events belonging to $\leq$8-pronged topologies, obtained in a 30,000 picture exposure of the ANL/NAL 30-inch bubble chamber to 102 GeV/c protons. All tracks from these events were measured in three views using standard 2.5μ least-count digitizing stages. A special program was written to match the tracks prior to their spatial reconstruction using the TVGP system.[1] All distributions have been corrected for measurement losses by weighting the events by the known topological cross sections.[2]

Single-Particle Spectra

Corrections for K^- and $\bar{p}$ contamination in the π^- spectra, as well as for K^+ and high-momentum proton contamination in the π^+ spectra were applied to the single particle inclusive data. These corrections were made by generating, through a Monte Carlo program, $K^\pm$ spectra according to the observed K^o_s data.[3] The energies of the generated $K^\pm$ tracks were subsequently changed by altering the mass hypothesis to that of a $\pi^\pm$. These spectra were subtracted from the measured negative and positive particle distributions. We used a $K^+(K^-)$ production cross section equal to 1.2(0.8) times the observed K^o_s cross section. The $\bar{p}$ contribution was taken to be 20% of the K^- yield. The proton subtraction was performed by extrapolating the measured proton spectrum for momenta below 1.2 GeV/c [5] in the reaction

$$pp \rightarrow p + \text{anything} \quad . \qquad (1)$$

We assumed that the differential cross section $\frac{d\sigma}{dx}$ (where x is the Feynman variable p^*_ℓ/p^*_o, and p^*_ℓ and p^*_o are respectively the longitudinal momentum of the final-state proton and the incident proton in the center of mass

system) for $-0.5 < x < 0.8$ was constant and equal to the observed value 15 ± 3 mb for $-0.8 < x < -0.5$. We assumed that proton production for $x > 0.8$ to be equal to that at $x < -0.8$, and used a Monte Carlo program to generate and misinterpret the fast protons as π^+ mesons and thus corrected the positive-track spectra.

All errors on the single-particle distributions presented contain both statistical and systematic uncertainties. The corrections to the negative spectra were typically of the order of 5% while the corrections to the positive-particle distributions were as large as 15% near $x \simeq 0$.

Figure 1 displays the distributions in the rapidity $y_{cm} = \frac{1}{2}\ell n(\frac{E^* + p_\ell^*}{E^* - p_\ell^*})$ for the π^+ and π^- data, integrated over transverse momenta (p_T) and summed over all topologies. For comparison we show similar data for π^- production at 12 and 24 GeV/c.[6] The latter are plotted in terms of the laboratory rapidity (E and p_ℓ are measured in the laboratory) in order to compare the three sets of data in the region of proton fragmentation. We note that all three π^- spectra overlap for $y_{LAB} \lesssim 0.5$, at which point the higher energy data start deviating from the 12 GeV/c and 24 GeV/c distributions. Thus the <u>inclusive</u> π^- cross section, for $y_{LAB} < 0.5$, has apparently reached its asymptotic limit below 12 GeV/c.

In Fig. 2 we display $d\sigma/dp_T^2$ for π^- produced in the backward hemisphere of the center of mass. For comparison we show data for the same reaction at 28.5 GeV/c.[7] The growth of this cross section reflects the rise of the π^- multiplicity with incident energy. However, aside from an overall rise in the cross section, there is also an apparent change in the shape of the p_T distribution due to an additional growth of the cross section for $p_T \gtrsim 1$ GeV/c. The average value of p_T shows a slow but definite rise with energy.[8] For data in the range $p_T < 1.5$ GeV/c we find $\langle p_T \rangle = 0.34 \pm 0.01$ GeV/c and $\langle p_T^2 \rangle = 0.17 \pm 0.01$ (GeV/c)^2.

The correlation between y and p_T is displayed in Fig. 3. The rise in $\langle p_T \rangle$ as a function of y is partly due to a larger phase space available for π^- production with larger p_T values at small y_{cm}.

The dependence of the y spectrum on multiplicity is shown in Fig. 4. The higher multiplicities are, clearly, characterized by lower mean values of $|y|$.

Two-Particle Correlations

In Figs. (5)-(7) we display data pertaining to two-particle correlations for the reactions (2)-(5):

$$pp \to \pi^c \pi^c + \ldots \quad (2)$$

$$pp \to \pi^+ \pi^- + \ldots \quad (3)$$

$$pp \to \pi^+ \pi^+ + \ldots \quad (4)$$

$$pp \to \pi^- \pi^- + \ldots \quad (5)$$

where the (c) indicates no selection on the charge of the pion. Corrections for $K^\pm$, p, $\bar{p}$ contamination cannot be made in the manner that the single particle spectra were corrected. We have, however, removed all protons identifiable by ionization, and all tracks which had a measured value for the longitudinal momentum in the center of mass in excess of 4 GeV/c. This last selection removes most of the forward produced protons while removing only a small fraction (<5%) of the forward produced π^+. The resulting single particle spectra are shown in Fig. 5. The remaining $K^\pm$, $\bar{p}$ backgrounds and the asymmetry in the positive spectra (caused by the remaining proton background) do not seriously affect the shapes or magnitudes of the correlations to be presented.

In Figs. 6(a,b,c,d) we show the double differential cross section for reactions (2)-(5). As $|y_1|$ increases there appears to be a trend for the y_2 distribution to fall and get wider. To improve the sensitivity to small changes in the shape and magnitude of the two-particle spectra we display in Figs. 7(a,b,c,d) the now standard correlated rapidity density for reactions (2)-(5). This density is defined as:

$$R_{12} = \frac{\sigma_{INEL} \frac{d^2\sigma}{dy_1\, dy_2}}{\frac{d\sigma}{dy_1}\frac{d\sigma}{dy_2}} - 1$$

where $\sigma_{INEL} = 31.9 \pm 0.8$ mb is the total inelastic cross section.[2]

The smooth curves shown in Figs. 7(a,b,c,d) represent the results of a pion-production model having the following properties:

(a) The <u>a priori</u> probabilities of each pion being a π^+, a π^-, or a π^o are equal, as are those for each nucleon being a neutron or a proton. Charge and baryon conservation alone are used to determine which final states are possible. The probability for the production of any particular number of pions is obtained by constraining the resultant charged particle multiplicity for the model to agree with that observed for the data.[2]

(b) The pions are produced with a cutoff transverse momentum distribution of the form $e^{-\alpha P_T^2}$, which is in approximate agreement with the data. The rapidity distribution of the generated pions is also chosen to be gaussian in shape, with a variance which decreases with total pion multiplicity as $1/\sqrt{n}$ (also in approximate agreement with the data), and with an overall scale factor which was chosen so that on the average the total energy carried away by all of the pions in an event amounts to one half the total center-of-mass energy.

The intent of the model was to compare the experimental data with a "control sample" of the same general kinematic character. In addition, we wished to investigate the effect of the multiple entering of events characterizing the calculation of correlation functions such as R_{12}. Although the nature of this comparison can at best only be semi-quantitative, the following general observations can be made:

(a) The R_{12} parameters for $\Delta y = 0$ are consistently larger than expected on the basis of our model. This is true for all charge configurations. In particular, simple Mueller-Regge ideas predict the absence of $\pi^+\pi^+$ and $\pi^-\pi^-$ correlations near $y_1 \approx y_2 \approx 0$,[9] whereas we observe relatively large values of $R_{12} \approx 0.4$.

(b) The magnitude of R_{12} for pions of all charge (Fig. 7a) agrees well with that observed for the central region of pion production at 205 GeV/c [10] and at ISR energies.[11] A similar statement can be made concerning the comparison of our results for $\pi^-\pi^-$ correlations (Fig. 7 d) with data for the same process at 303 GeV/c.[12] Thus the maxima in R_{12} appear to be essentially energy independent.

(c) The model does not reproduce the magnitude or shape of R_{12}, particularly for the $\pi^+\pi^-$ data. This is most evident when the two particles are produced away from the most central region. The observed correlations for $\Delta y = 0$ can be taken as evidence for particle clustering in the production process, a possibility not explicitly put into our model.

Transverse momentum correlations (the azimuth angle between transverse momenta of two particles defined as:

$$\cos \phi = \vec{P}_T^{\,1} \cdot \vec{P}_T^{\,2} / \left(|P_T^1| \, |P_T^2| \right)$$

are shown in Fig. 8. The results are for events with six or more charged

prongs. Again we note that the data for unlike-charged pions appear to show more structure than for pions of same charge. Here, however, momentum conservation requires some anti-correlation and, consequently, the lack of correlation in reactions (4) and (5), and the reduced correlation in reaction (3) for large rapidity gaps between the two pions, would appear to have a dynamic origin.[13] For example, it may be that pions of like charge frequently have other (charged or neutral) pions between them in the rapidity chain. The diminution in the azimuthal correlation for large rapidity difference may be related to the nature of the Pomeranchuk trajectory.[14]

Forward/Backward Correlations in the Center of Mass

The charge transfer distribution, i.e., half the difference between the charge moving in the forward direction (Q_F) and in the backward direction in the center of mass (Q_B) is shown in Fig. 9a. (There is a very slight asymmetry in the data due to misidentification of protons.) The variance of the distribution, $\langle u^2\rangle=\frac{1}{4}\langle(Q_F-Q_B)^2\rangle$ has bearing on the nature of the production mechanism.[15] We find $\langle u^2\rangle=0.90\pm0.04$. This variable has a weak dependence on laboratory momentum (Fig.9 b), which is more in line with predictions based on a multiperipheral mechanism than with those afforded by a fragmentation or fireball model.[15]

Finally, in Fig.10a we plot the average multiplicity in the forward hemisphere $\langle n_F\rangle$ as a function of the number of particles emitted backward in the center of mass frame (n_B). We note that there is a weak positive correlation between n_B and $\langle n_F\rangle$ for all multiplicities. The effect of the low-multiplicity diffractive contribution is discernible in the dips observed for n_B=1 and 3. In particular, the 4-pronged topology exhibits a strong preference for a separation of 1 charged particle into one hemisphere of the center of mass and 3 into the other (Fig.10b), whereas the higher topologies (Figs.10c,d) show a smooth behavior as a function of n_B.

We thank the members of the NAL Neutrino Laboratory, the Accelerator Operations Group and the Liason Staff for aid in obtaining our film exposure. We also thank our diligent scanning and measuring personnel for their outstanding cooperation.

References

1. The details will be available in C. Bromberg, Ph. D. Thesis, University of Rochester. For general information see P. Slattery in Proceedings of 1973 Vanderbilt Conference, AIP Conference No. 12, R. S. Panvini, ed.

2. Only about 10% of the events were not measureable in the greater than 12-pronged topologies. In the lower multiplicity classes these losses were of the order of 3%. For the latest inelastic and topological cross sections see the Michigan-Rochester Report UMBC 73-18,UR-459(to be published).

3. See the Michigan-Rochester report of A. Seidl et al., UMBC 73-20, UR-457 (to be published).

4. These corrections tend to underestimate the K^+ contamination away from the central region of pion production. For more details see reference 1 and the report of J. Whitmore appearing in the Proceedings of the 1973 Vanderbilt Conference, AIP Conference No. 12, R. S. Panvini, ed.,and M.Antinucci et al.,Lett.Nuovo Cimento 6,121(1973).

5. See the Michigan-Rochester Group report of C. Bromberg et al., UMBC 72-14, UR-416, and the report in preparation UMBC 73-21, UR-458 (to be published).

6. H. J. Mück et al., DESY Report F1-72/1. These data are statistically superior to our results and have consequently been smoothed for convenient comparison.

7. W. H. Sims et al., Nuclear Physics B41, 317 (1972).

8. See for comparison the study of J. Anderson et al., University of Rochester Report, UR-433 (to appear in Physics Letts.) and T. Ferbel, Proceedings of the International Symposium on High Energy Physics (Tokyo, 1973).

9. See C. Quigg in Proceedings of the 1973 Vanderbilt Conference, AIP Conference No. 12, R. S. Panvini, ed.

10. R. Engelmann et al., ANL/HEP 73-41.

11. G. Belletini, Proceedings of the International Conference on High Energy Physics at Chicago/NAL (1972). J. D. Jackson and A. Roberts,eds.

12. Preprint from the 30-inch Hybrid Spectrometer Group, B. Y. Oh et al., (abstract #38 submitted to Berkeley 1973 DPF Meeting).

13. For comparison see the low-energy results given in S. Stone et al., Phys. Rev. D5, 1621 (1972),and M.C.Foster et.al.,Phys.Rev.D6,3135(1972).

14. See, for example, D. Z. Freedman et al., Phys. Rev. Letters 26, 1197 (1971), and references given therein.

15. See references given in J. Whitmore, op. cit.

Figure Captions

Fig. 1. The rapidity spectrum integrated over transverse momentum for π^+ and π^- mesons produced in proton-proton collisions at 102 GeV/c. Also shown are smooth curves representing data for π^- production at 12 and 24 GeV/c as a function of laboratory rapidity.

Fig. 2. The transverse momentum spectrum for backward π^- produced in the center of mass. Also shown is a smooth curve representing the data for the same reaction at 28.5 GeV/c.

Fig. 3. The mean transverse momentum for π^- mesons as a function of the rapidity in the center of mass system.

Fig. 4. The rapidity spectra for π^- mesons produced in various topological classes.

Fig. 5. The rapidity spectra for the positive and negative particles used in the calculation of the two-pion rapidity correlations. Protons have been removed using the procedure described in the text.

Fig. 6. The two particle rapidity spectra in the reactions (a) $pp \to \pi^c\pi^c + \ldots$, (b) $pp \to \pi^+\pi^- + \ldots$, (c) $pp \to \pi^+\pi^+ + \ldots$, (d) $pp \to \pi^-\pi^- + \ldots$, for the rapidity intervals used in the calculation of the two-particle correlations. For clarity the data points have been displaced to the left (dark points) and to the right (open circles) of the central rapidity value in each bin.

Fig. 7. The two particle correlated rapidity density R_{12} plotted as a function of the difference between the rapidities of the two pions in the reactions (a) $pp \to \pi^c\pi^c + \ldots$, (b) $pp \to \pi^+\pi^- + \ldots$, (c) $pp \to \pi^+\pi^+ + \ldots$, (d) $pp \to \pi^-\pi^- + \ldots$. The results of the model described in the text are to be compared with the dark data points.

Fig. 8. The frequency for observing two pions with an angle ϕ between the transverse momenta (each plot is normalized to an average height of 1). The data are subdivided into pion charge states and into rapidity-difference intervals. The dashed curves are the results of the pion-production model described in the text. Protons and events with less than 6 charged particles have been removed.

Fig. 9. (a) The cross section for observing an amount of charge, u, to be transferred from the backward to the forward hemisphere in the center of mass, and (b) the variance of the charge transfer distribution as a function of the incident momentum in proton-proton collisions. Also shown are the predictions characteristic of fragmentation and multiperipheral models (private communication from C. Quigg).

Fig.10. (a) The mean number of charged particles observed in the forward hemisphere of the center of mass, $\langle n_F \rangle$, as a function of the number of charged particles observed in the backward hemisphere (n_B). (b-d) The cross section for observing n_B charged particles in the backward hemisphere of the center of mass for the topological classes N = 4,6,8 prongs.

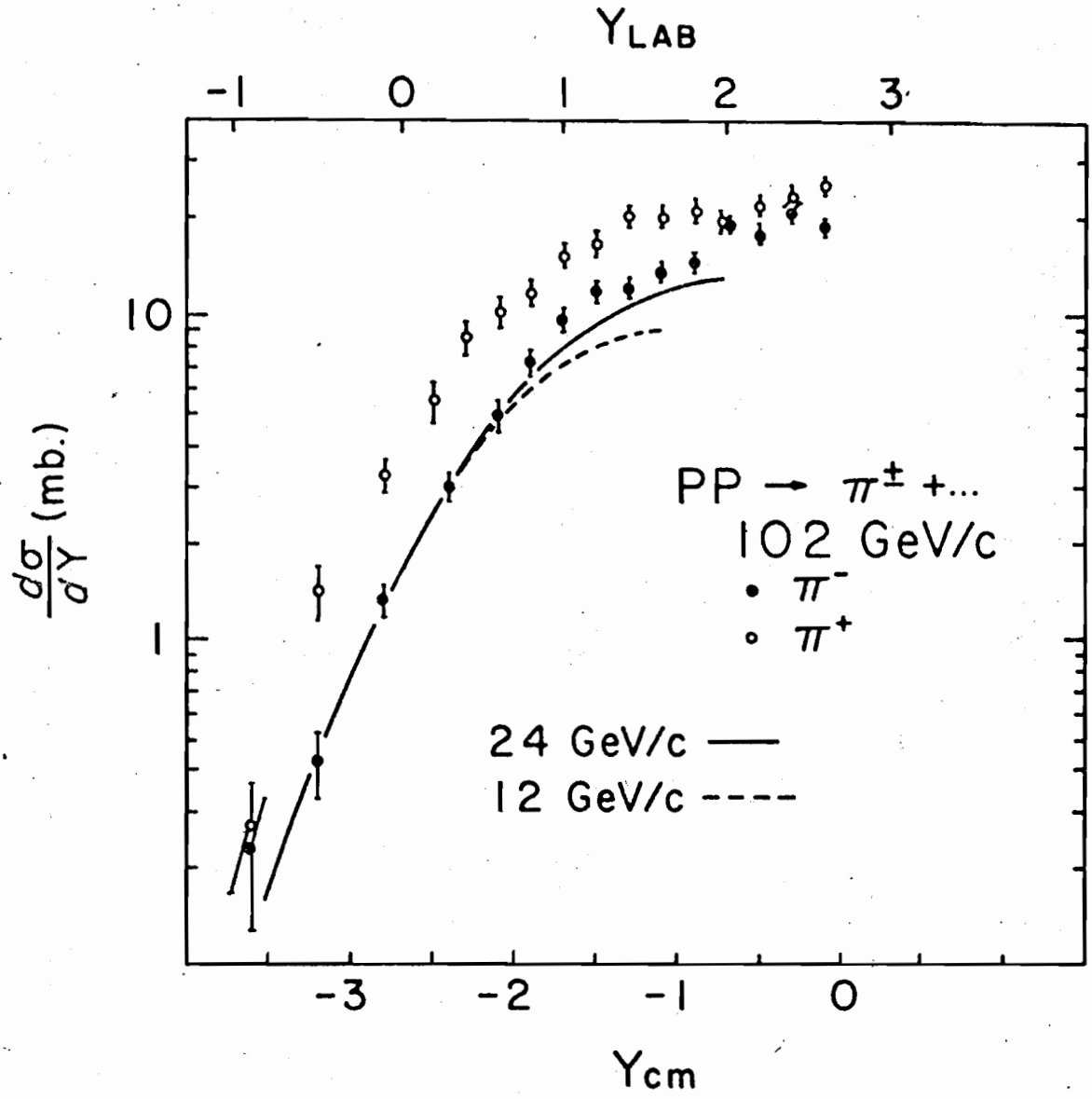
Y_{LAB}
-1
0
1
2
3
10
1
$\frac{d\sigma}{dY}$ (mb.)
$PP \rightarrow \pi^{\pm} + \ldots$
102 GeV/c
$\bullet\ \pi^-$
$\circ\ \pi^+$
24 GeV/c
12 GeV/c
-3
-2
-1
0
Ycm

Fig. 1

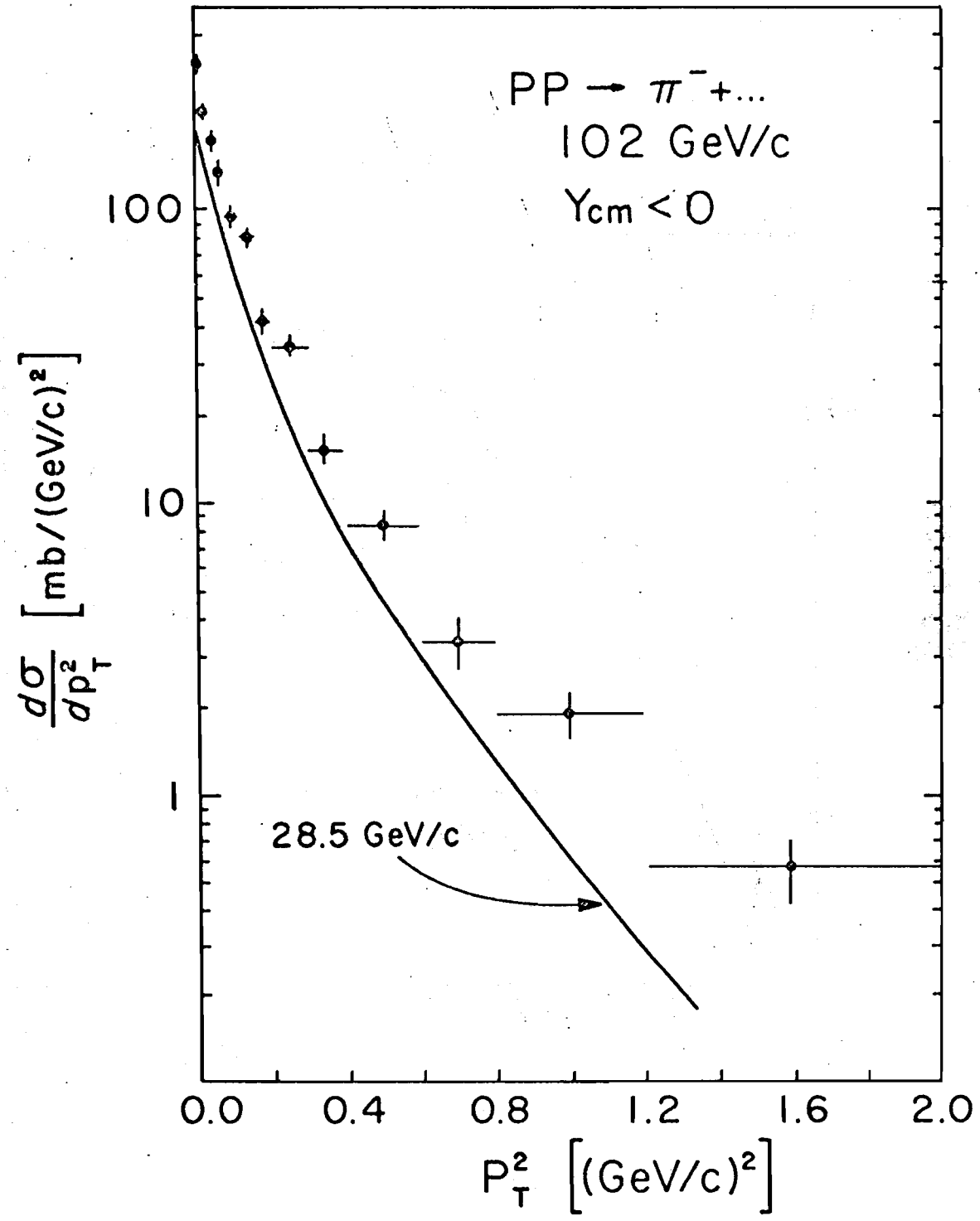
PP → π⁻+...
102 GeV/c
Ycm < 0
100
10
1
28.5 GeV/c
dσ/dp²T [mb/(GeV/c)²]
0.0
0.4
0.8
1.2
1.6
2.0
P²T [(GeV/c)²]

Fig. 2

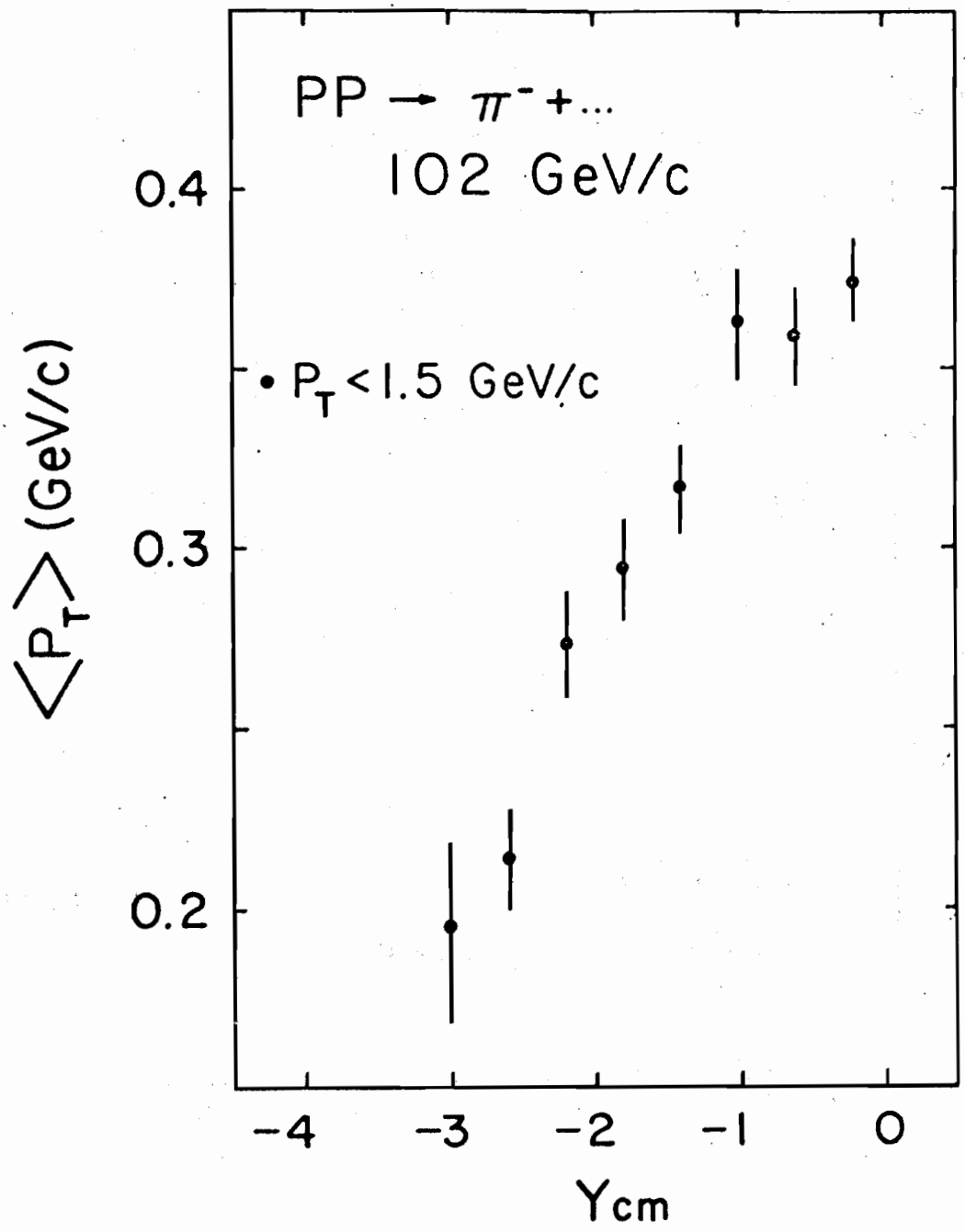

Fig. 3

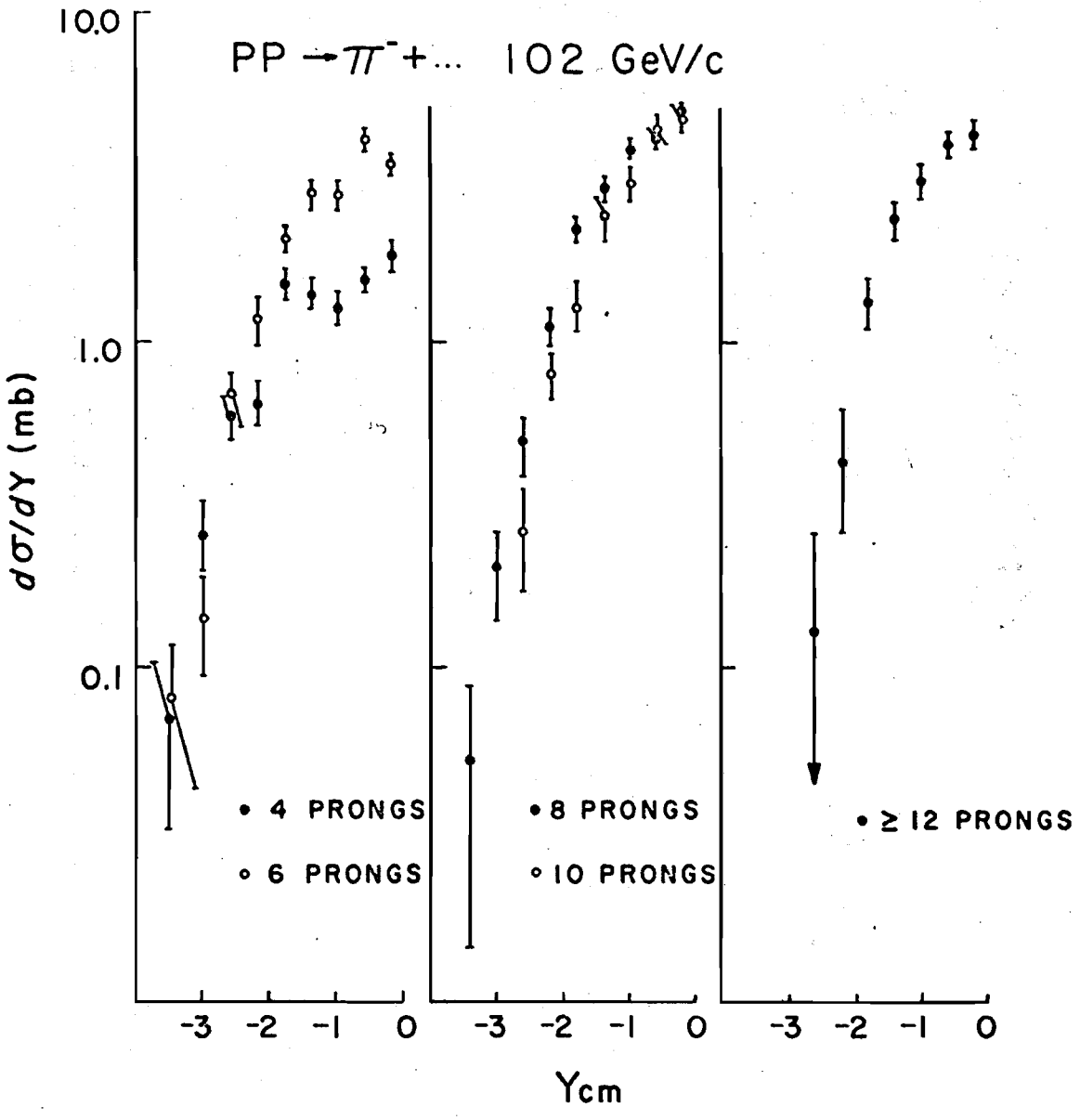
PP → π⁻ + ... 102 GeV/c
10.0
1.0
0.1
dσ/dY (mb)
• 4 PRONGS
○ 6 PRONGS
• 8 PRONGS
○ 10 PRONGS
• ≥ 12 PRONGS
-3 -2 -1 0
Ycm

Fig. 4

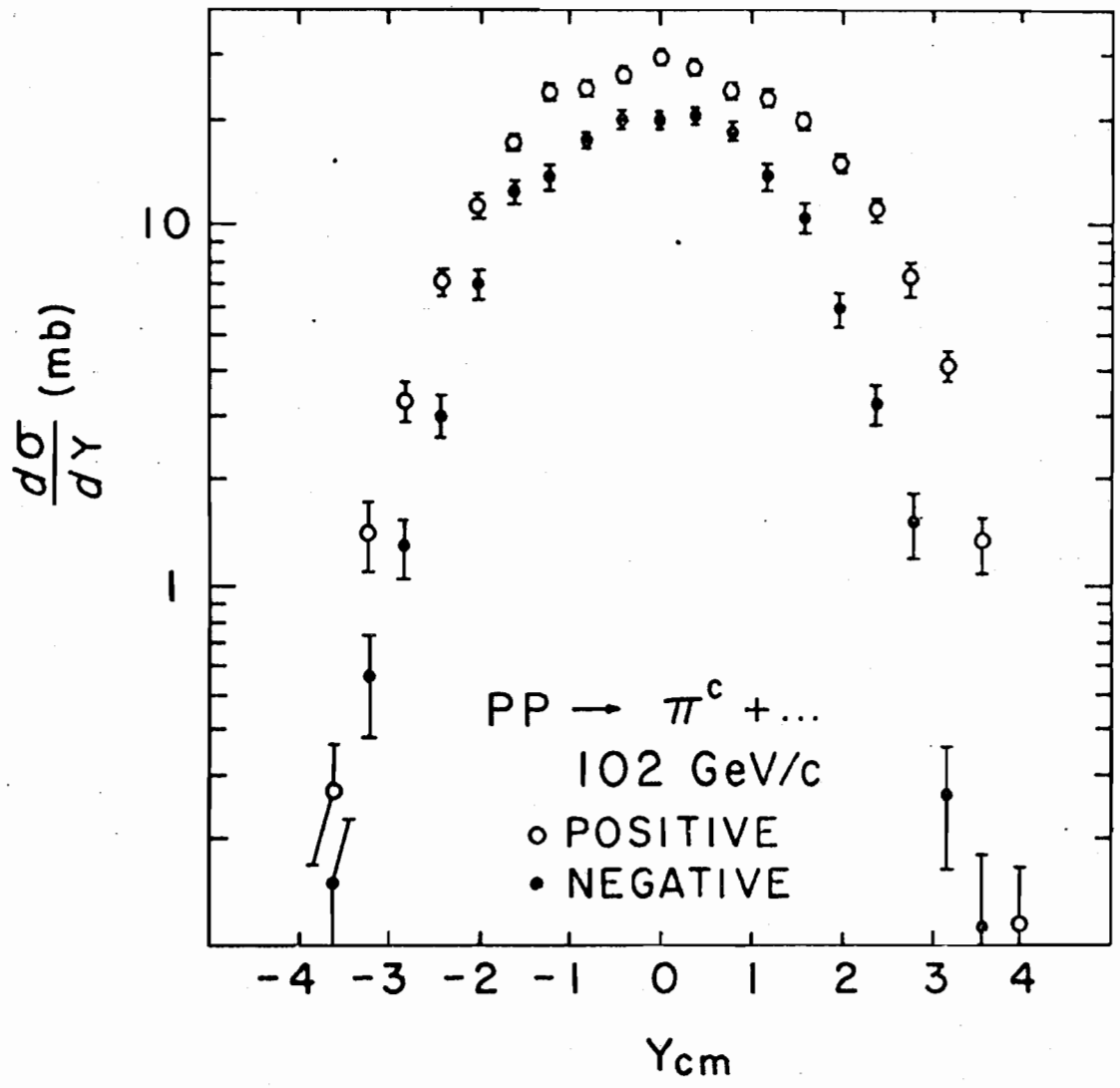
$\frac{d\sigma}{dY}$ (mb)
10
1
PP → π^c + ...
102 GeV/c
o POSITIVE
• NEGATIVE
-4 -3 -2 -1 0 1 2 3 4
Ycm

Fig. 5

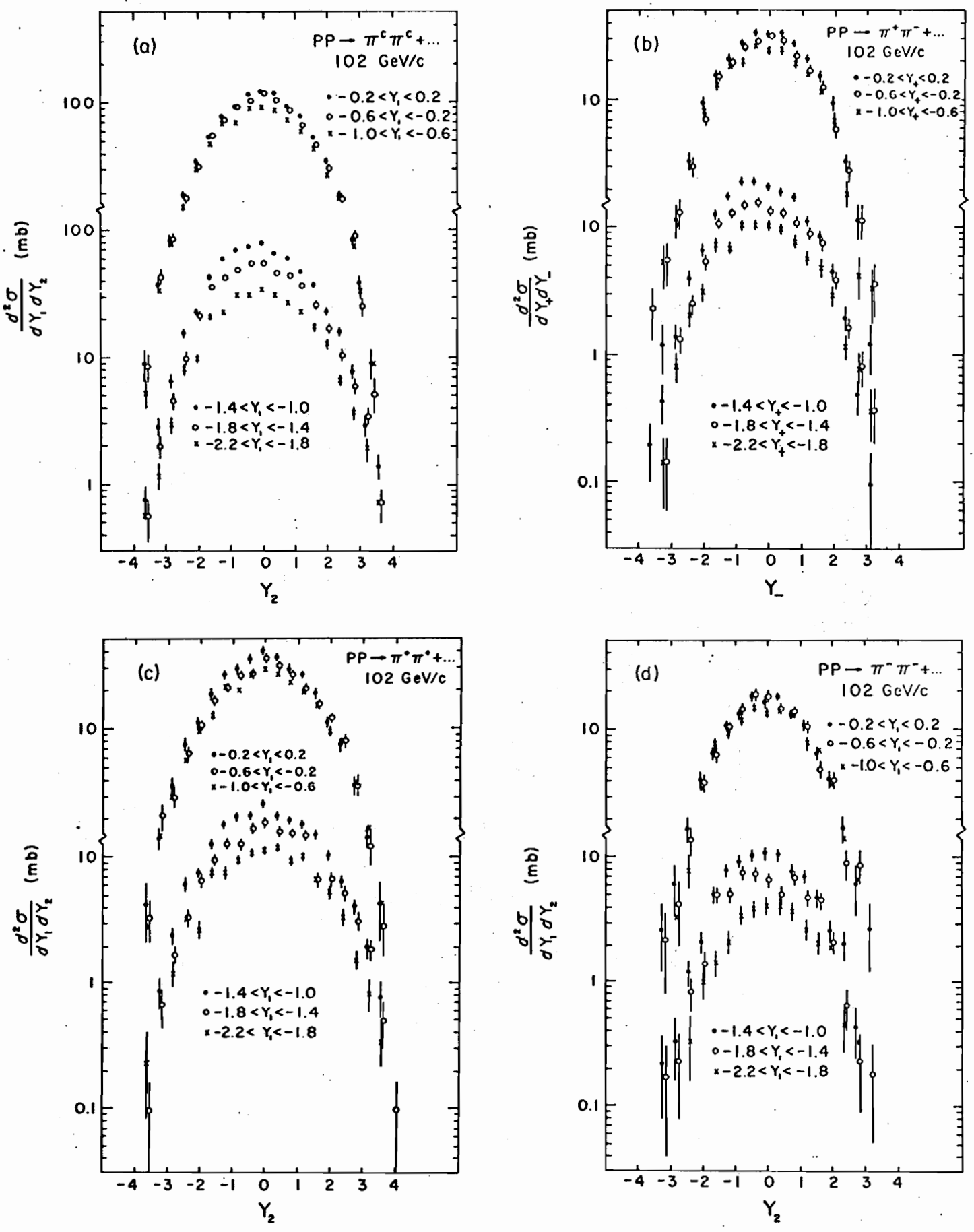
(a)
PP → π^c π^c +...
102 GeV/c
• -0.2<Y1<0.2
o -0.6<Y1<-0.2
x -1.0<Y1<-0.6
• -1.4<Y1<-1.0
o -1.8<Y1<-1.4
x -2.2<Y1<-1.8
d²σ/dY1 dY2 (mb)
Y2
(b)
PP → π⁺π⁻+...
102 GeV/c
• -0.2<Y+<0.2
o -0.6<Y+<-0.2
x -1.0<Y+<-0.6
• -1.4<Y+<-1.0
o -1.8<Y+<-1.4
x -2.2<Y+<-1.8
d²σ/dY+dY- (mb)
Y-
(c)
PP → π⁺π⁺+...
102 GeV/c
• -0.2<Y1<0.2
o -0.6<Y1<-0.2
x -1.0<Y1<-0.6
• -1.4<Y1<-1.0
o -1.8<Y1<-1.4
x -2.2< Y1<-1.8
d²σ/dY1 dY2 (mb)
Y2
(d)
PP → π⁻π⁻+...
102 GeV/c
• -0.2<Y1<0.2
o -0.6<Y1<-0.2
x -1.0<Y1<-0.6
• -1.4<Y1<-1.0
o -1.8<Y1<-1.4
x -2.2<Y1<-1.8
d²σ/dY1 dY2 (mb)
Y2

Fig. 6

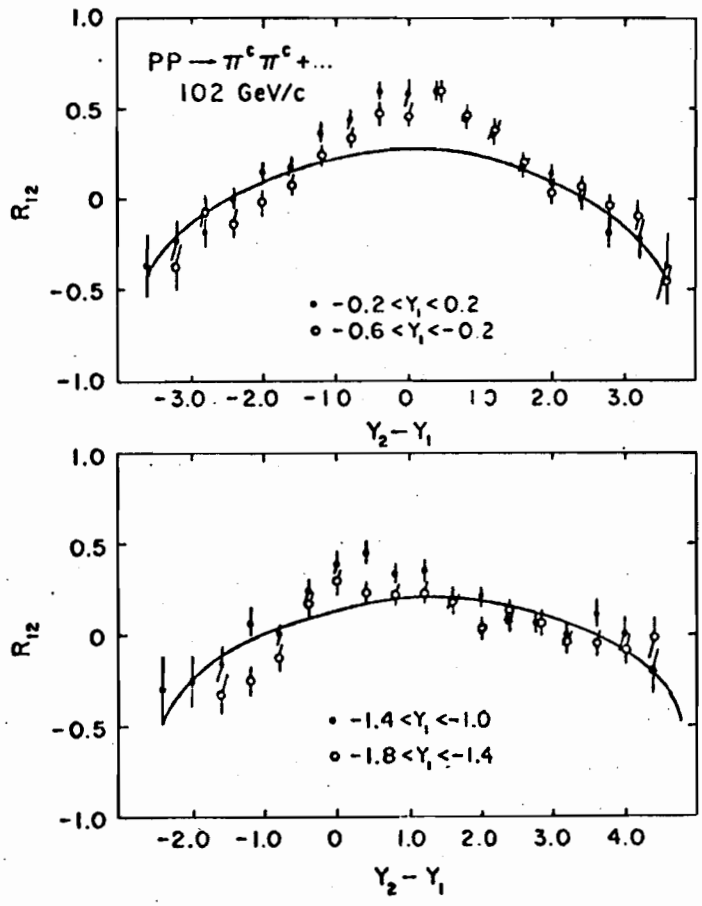
PP → π^c π^c +...
102 GeV/c
• -0.2 < Y_1 < 0.2
o -0.6 < Y_1 < -0.2
R_12
Y_2 − Y_1
• -1.4 < Y_1 < -1.0
o -1.8 < Y_1 < -1.4

(a)

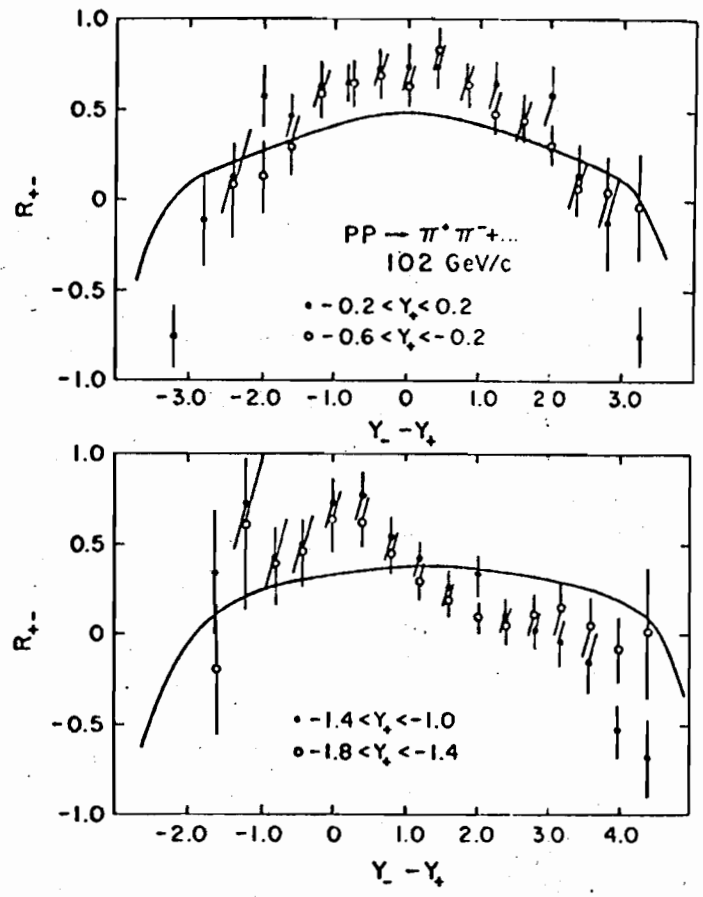
PP → π⁺ π⁻ +...
102 GeV/c
• -0.2 < Y_+ < 0.2
o -0.6 < Y_+ < -0.2
R_+-
Y_- − Y_+
• -1.4 < Y_+ < -1.0
o -1.8 < Y_+ < -1.4

(b)

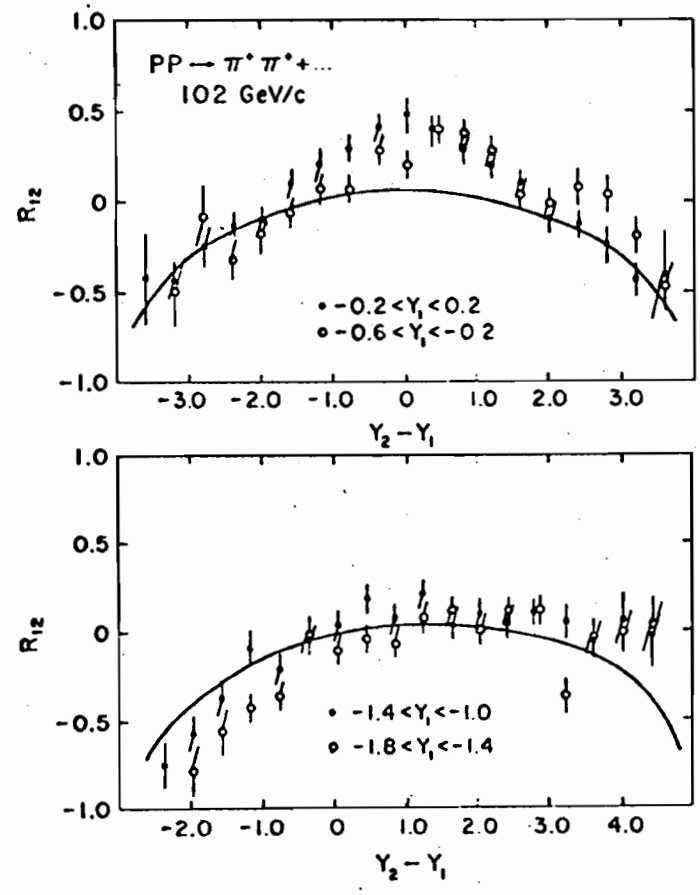
PP → π⁺ π⁺ +...
102 GeV/c
• -0.2 < Y_1 < 0.2
o -0.6 < Y_1 < -0.2
R_12
Y_2 − Y_1
• -1.4 < Y_1 < -1.0
o -1.8 < Y_1 < -1.4

(c)

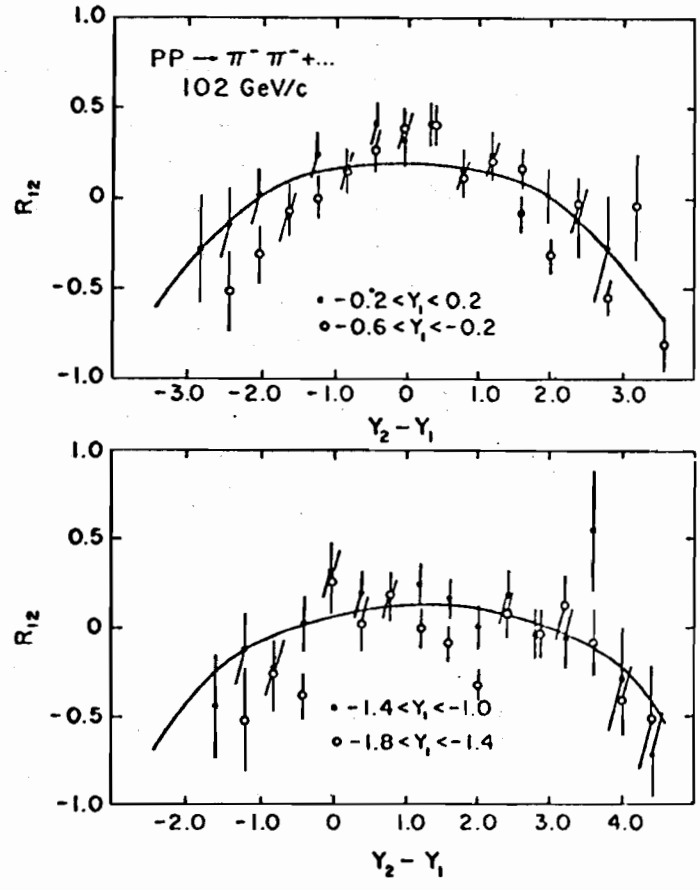
PP → π⁻ π⁻ +...
102 GeV/c
• -0.2 < Y_1 < 0.2
o -0.6 < Y_1 < -0.2
R_12
Y_2 − Y_1
• -1.4 < Y_1 < -1.0
o -1.8 < Y_1 < -1.4

(d)

Fig. 7

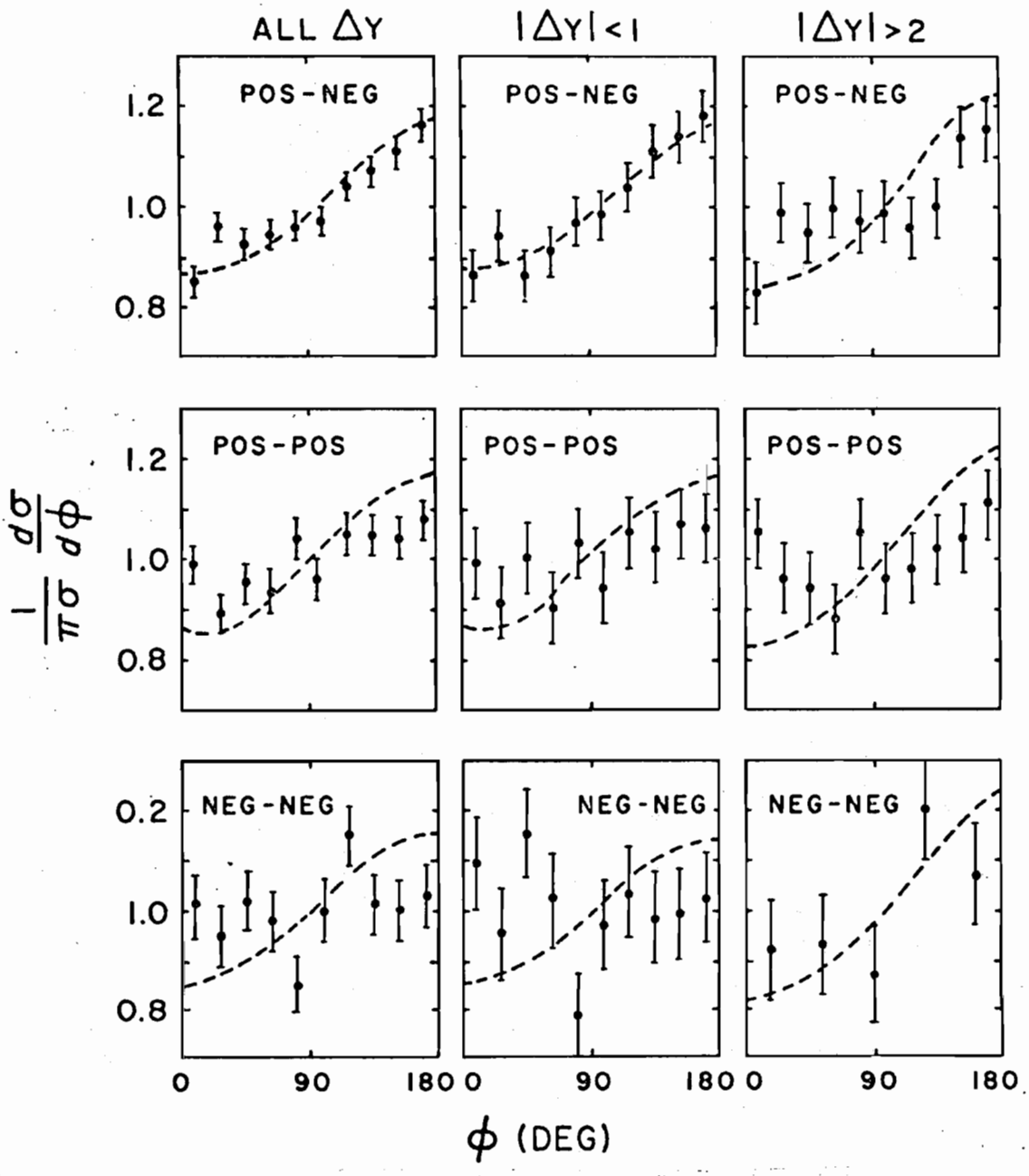
ALL ΔY
|ΔY|<1
|ΔY|>2
POS-NEG
POS-POS
NEG-NEG
1.2
1.0
0.8
0.2
0
90
180
$\frac{1}{\pi\sigma}\frac{d\sigma}{d\phi}$
ϕ (DEG)

Fig. 8

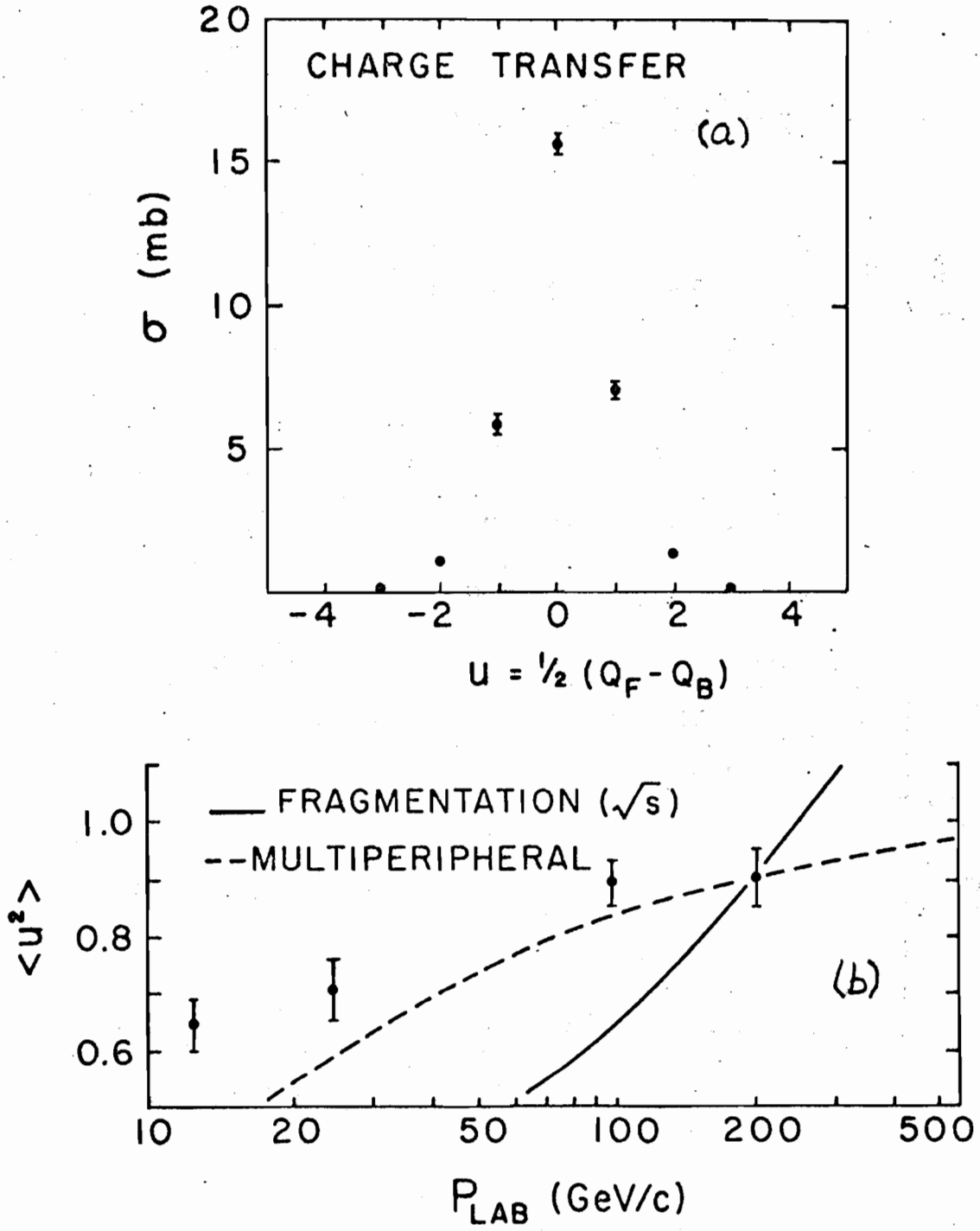
CHARGE TRANSFER
(a)
σ (mb)
20
15
10
5
-4
-2
0
2
4
u = ½ (Q_F - Q_B)
FRAGMENTATION (√s)
--MULTIPERIPHERAL
(b)
<u²>
1.0
0.8
0.6
10
20
50
100
200
500
P_LAB (GeV/c)

Fig. 9

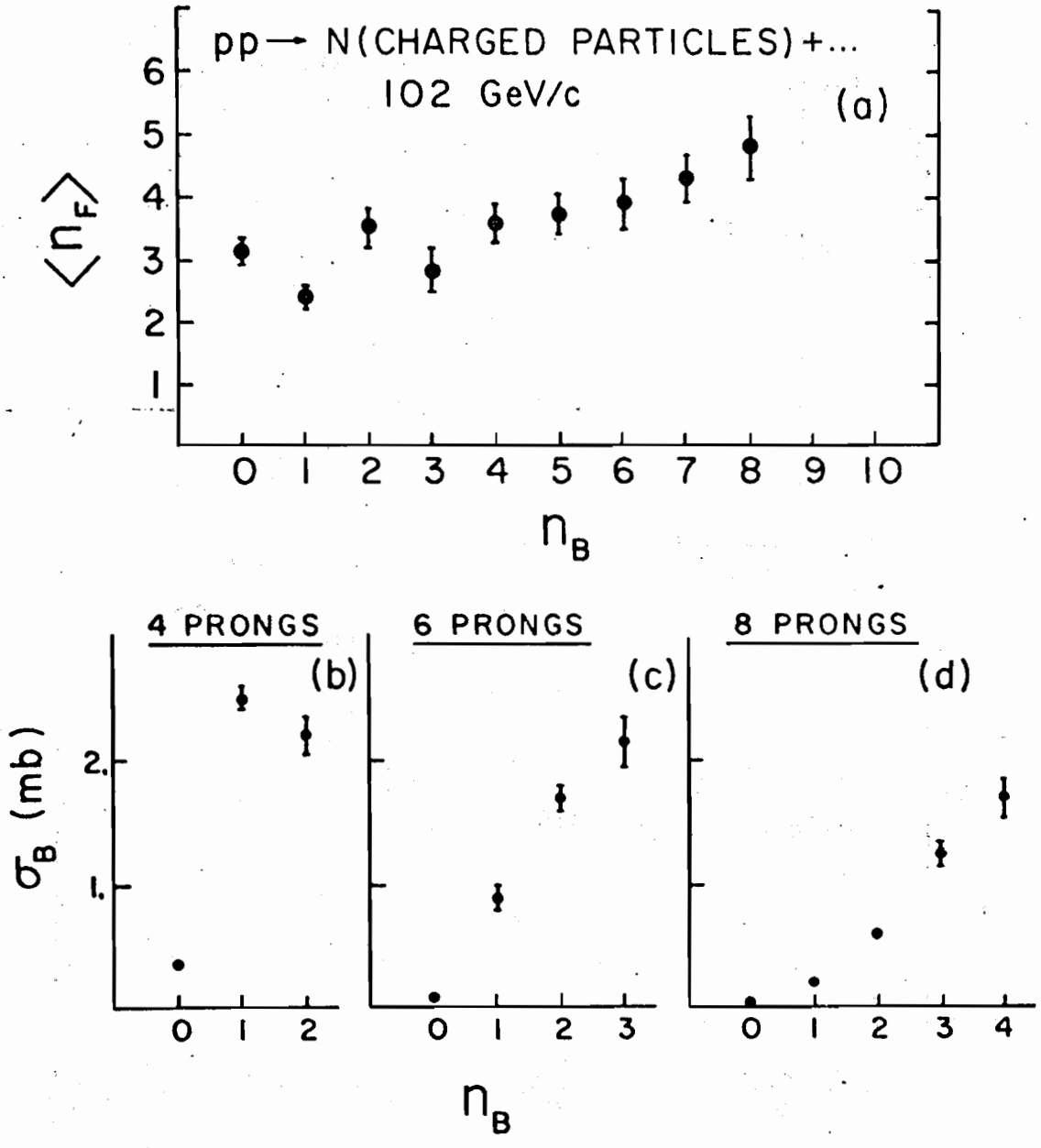
pp → N(CHARGED PARTICLES)+...
102 GeV/c
(a)
$\langle n_F \rangle$
n_B
4 PRONGS
(b)
6 PRONGS
(c)
8 PRONGS
(d)
σ_B (mb)
n_B

Fig. 10